QUANTUM COMPUTING

Deterministic generation of a two-dimensional cluster state

Mikkel V. Larsen*, Xueshi Guo, Casper R. Breum, Jonas S. Neergaard-Nielsen, Ulrik L. Andersen*

Measurement-based quantum computation offers exponential computational speed-up through simple measurements on a large entangled cluster state. We propose and demonstrate a scalable scheme for the generation of photonic cluster states suitable for universal measurement-based quantum computation. We exploit temporal multiplexing of squeezed light modes, delay loops, and beam-splitter transformations to deterministically generate a cylindrical cluster state with a two-dimensional (2D) topological structure as required for universal quantum information processing. The generated state consists of more than 30,000 entangled modes arranged in a cylindrical lattice with 24 modes on the circumference, defining the input register, and a length of 1250 modes, defining the computation depth. Our demonstrated source of two-dimensional cluster states can be combined with quantum error correction to enable fault-tolerant quantum computation.

Quantum computing represents a new paradigm for information processing that harnesses the inherent nonclassical features of quantum physics to find solutions to problems that are computationally intractable on classical processors (*1*). In measurement-based, or cluster state, quantum computing (MBQC), the processing is performed by simple single-site measurements on a large entangled cluster state (*2*). This constitutes a simplification over the standard gate-based model of quantum computing, as it replaces complex coherent unitary dynamics with simple projective measurements. However, one of the outstanding challenges in realizing cluster state computation is the reliable, deterministic, and scalable generation of nonclassical entangled states suitable for universal information processing.

Several candidate platforms for scalable cluster state generation have been proposed and some experimentally realized, including solid-state superconducting qubits (*3*), trapped ion qubits (*4*, *5*), and photonic qubits or qumodes, in which qubits can be encoded, generated by parametric down-conversion (*6*–*9*) or by quantum dots (*10*). However, none of these implementations has demonstrated true scalability combined with computational universality. The largest cluster state generated to date is a temporally multiplexed photonic state comprising entangled modes in a long chain, which, however, does not allow for universal computation because of its one-dimensional (1D) topological structure (*8*, *11*). To achieve universality, the dimension of the cluster state must be at least two. Several proposals for generating 2D cluster states in different systems have been proposed (*12*–*15*), but owing to technical challenges, scalable and computationally universal cluster states have yet to be produced in any physical system.

We propose and demonstrate a highly scalable scheme for the generation of cluster states for universal quantum computation based on quantum continuous variables (CVs) where information is encoded in the position or momentum quadratures of photonic harmonic oscillators (*16*). We use a temporally multiplexed source of optical Einstein-Podolsky-Rosen (EPR) states (*17*) to generate a long string of entangled modes that is curled up and fused to form a 2D cylindrical array of entangled modes. Specifically, we generate a massive cluster state of more than 30,000 entangled modes comprising an input register of $2 \times 12 = 24$ modes on which the input state may be encoded, and a length of 1250 modes for encoding operations by projective measurements, limited only by the phase stability of our setup. In addition to being universal and deterministically generated, the source is operated under ambient conditions in optical fibers at the low-loss telecom wavelength of 1550 nm. These favorable operational conditions and specifications facilitate further upscaling of the entangled state, as well as its use in applications and fundamental studies.

The canonical approach to CV cluster state generation is to apply two-mode controlled-Z gates onto pairs of individually prepared eigenstates of the momentum (or phase quadrature) operators $\hat{p}_i, \hat{p}_j$ in adjacent modes i, j. The gate is described by the unitary operation $\hat{C}_Z = e^{ig\hat{x}_i\hat{x}_j}$, where $\hat{x}_i, \hat{x}_j$ are the position (amplitude quadrature) operators of mode i and j, and g is the interaction strength. Applying this gate to two modes leads to entanglement in the form of quantum correlations of the two modes' quadratures. The operations and resulting state can be represented by a graph in which the nodes represent the momentum eigenstates and the edges (links) between the nodes represent the application of a controlled-Z operation, where the interaction strength is given by the edge weight. In a practical implementation, the unphysical momentum eigenstates are replaced by highly squeezed states, while the controlled-Z operations can be imitated by phase shifts and beam-splitter transformations. To enable scalability, it has been suggested that multiplexing of spatial modes (*18*), frequency modes (*19*, *20*), or temporal modes (*13*, *21*) be used. For example, Menicucci suggested using temporal multiplexing to form a 2D cluster state combining four squeezed state generators, five beam splitters, and two delay lines (*13*).

We propose a simpler approach to 2D cluster state generation that lowers the experimental requirements (Fig. 1). The state is produced in four steps: (i) Pairs of squeezed vacuum states are generated at 1550-nm wavelength from two bowtie-shaped optical parametric oscillators (OPOs) by parametric down conversion (*22*). The states are defined in consecutive temporal modes of duration τ of the continuously generated OPO output. (ii) The squeezed vacuum pairs in spatial modes A and B are interfered on a balanced beam splitter (denoted BS_1). This produces a train of pairwise EPR-entangled temporal modes that exhibit quantum correlation between the position and momentum quadratures. Each EPR pair can be represented by a simple graph of a single edge connecting two nodes. (iii) A 1D cluster state is formed by delaying one arm of the interferometer by τ with respect to the other arm and interfering the resulting time-synchronized modes on another balanced beam splitter (denoted BS_2). The interference entangles EPR pairs along an indefinitely long chain, creating a 1D graph. (iv) In the final step, the 2D cluster state is produced by introducing another delay to one interferometer arm of duration $N\tau$ and interfering the resulting time-synchronized modes on a final beam splitter (denoted BS_3). This effectively curls up the graph and fuses the modes into an indefinitely long cylinder with N nodes on the circumference, as illustrated in Fig. 1 for $N = 12$, leading to $2 \times N = 24$ input modes distributed on the two spatial modes A and B. For a detailed description of experimental implementations, see material and methods (*23*).

All states and operations involved are Gaussian, meaning they can be described by Gaussian distributions of the quadrature variables in phase space. In the formalism of graphical calculus for Gaussian states (*24*), the generated graphs are so-called H-graphs, as they can be generated from vacuum by a single Hamiltonian and have an edge weight of $g = i\sinh(2r)G$, where r is the squeezing parameter of the two squeezing operations and $G = -1$ for the EPR states, $\pm 1/2$ for the 1D graph, and $\pm 1/4, 1/2$ for the 2D graph. Owing to the particular structure

Center for Macroscopic Quantum States (bigQ), Department of Physics, Technical University of Denmark, Fysikvej, 2800 Kgs. Lyngby, Denmark.
*Corresponding author. Email: mivila@fysik.dtu.dk (M.V.L.); ulrik.andersen@fysik.dtu.dk (U.L.A.)

of the *H*-graph generated here [it is self-inverse and bipartite; see supplementary text section 1.1 for details (*23*)], it can be transformed into a cluster state by $\pi/2$ rotations in phase space, leading to real edges of weight $g = \tanh(2r)G \to G$ for $r \to \infty$. Finally, as the $\pi/2$ phase space rotations can be absorbed into the measurement basis, or simply by appropriate redefinitions of quadratures on the rotated modes, the generated *H*-graph state and its corresponding cluster state are completely equivalent. [See supplementary text section 1.2 for details on the cluster state generation scheme (*23*).]

The produced cylindrical 2D cluster state can be shown to be a universal resource for quantum computing: In Fig. 2, the generated cylindrical cluster state is unfolded and projected into a square lattice by projective measurements in the position basis and $\pi/2$ phase-space rotations of different modes. Such a square lattice is a well-known universal resource for quantum computing (*25*), and thus the initial cylindrical cluster state is itself universal. For computation, it is not necessary to project the generated cluster state into a square lattice—rather, one would in general optimize the detector settings required for the gate to be implemented. For instance, with proper settings, the cluster state can be projected into 1D dual-rail wires along the cylinder, an efficient resource for one-mode computation (*8*, *21*) and with possible two-mode interactions between them [for details, see supplementary text section 1.4 (*23*)]. Doing so requires fast control of the measurement bases in between temporal modes, whereas in this work, the cluster state is measured in fixed bases for state verification.

Multipartite cluster state inseparability can be witnessed through the measurement of the uncertainties of the state nullifiers—linear combinations of position and momentum operators for which the cluster states are eigenstates with eigenvalue 0. For example, for the ideal two-mode EPR state, the well-known nullifiers are $\hat{n}^x_{\mathrm{EPR}} = \hat{x}_A - \hat{x}_B$ and $\hat{n}^p_{\mathrm{EPR}} = \hat{p}_A + \hat{p}_B$ because $\hat{n}^x_{\mathrm{EPR}}|\mathrm{EPR}\rangle = 0$ and $\hat{n}^p_{\mathrm{EPR}}|\mathrm{EPR}\rangle = 0$. For our 2D cluster state, $|2\mathrm{D}\rangle$, the nullifiers consist of eight modes and are given by

$$\hat{n}^x_k = \hat{x}^A_k + \hat{x}^B_k - \hat{x}^A_{k+1} - \hat{x}^B_{k+1} - \hat{x}^A_{k+N} + \hat{x}^B_{k+N} - \hat{x}^A_{k+N+1} + \hat{x}^B_{k+N+1} \quad (1)$$

$$\hat{n}^p_k = \hat{p}^A_k + \hat{p}^B_k + \hat{p}^A_{k+1} + \hat{p}^B_{k+1} - \hat{p}^A_{k+N} + \hat{p}^B_{k+N} + \hat{p}^A_{k+N+1} - \hat{p}^B_{k+N+1} \quad (2)$$

as $\hat{n}^x_k|2\mathrm{D}\rangle = 0$ and $\hat{n}^p_k|2\mathrm{D}\rangle = 0$ [derived in supplementary text section 1.3 (*23*)], where the subscript indicates the temporal mode

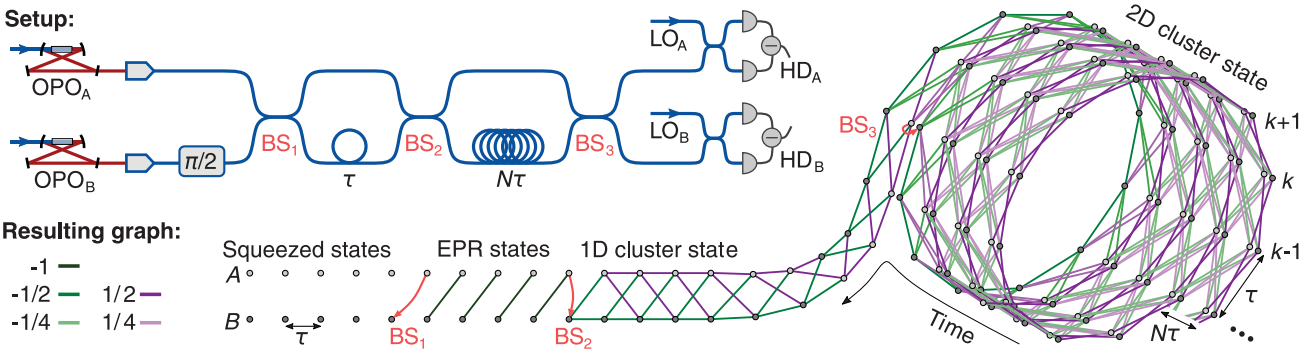

Fig. 1. Scheme of 2D cluster state generation. Squeezing is produced by two OPOs ($\mathrm{OPO_A}$ and $\mathrm{OPO_B}$), and coupled into fiber with 97% coupling efficiency. There, temporal modes are interfered with fiber-coupled beam splitters to generate a 2D cluster state. The corresponding graph is shown: Temporal modes of squeezing with mode index *k* in two spatial modes *A* and *B* (bright and dark nodes) are interfered to generate EPR states at $\mathrm{BS_1}$. The EPR pairs are entangled to form a 1D cluster state using a τ delay in mode *B* and $\mathrm{BS_2}$, and the 1D cluster state is curled up to a 2D cluster state by another delay of $N\tau$ and $\mathrm{BS_3}$. Using homodyne detectors ($\mathrm{HD_A}$ and $\mathrm{HD_B}$), the temporal mode quadratures are measured, from which the nullifiers are calculated. In the experimental implementation, the short delay is a 50.5-m fiber leading to temporal modes of 247-ns duration, whereas the long delay is a 606-m fiber such that $N = 12$, as shown in the illustrated graph. The temporal modes are defined by an asymmetric-shaped temporal mode function within the 247-ns duration, which filters out low-frequency noise and leads to less than 10^{-3} mode overlap (*11*). For more information, see material and methods (*23*).

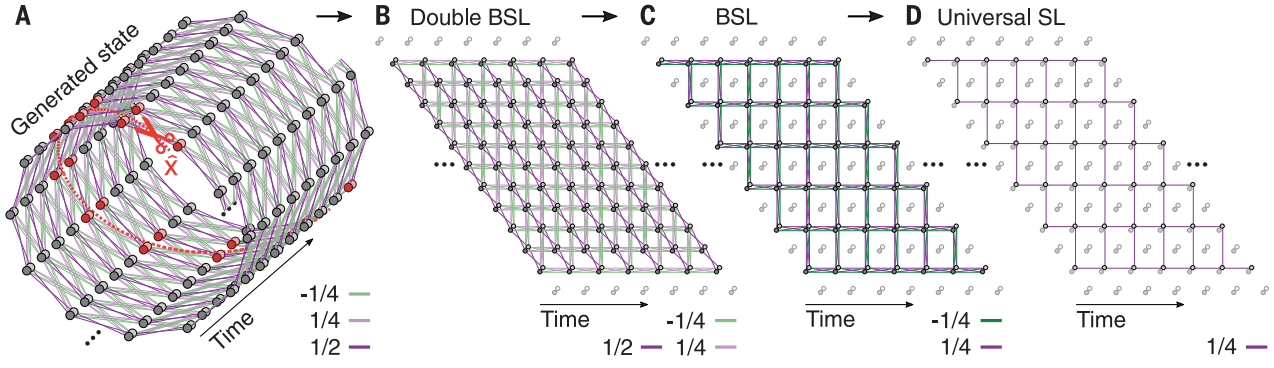

Fig. 2. Universality of the generated 2D cluster state. (**A**) Graph of the generated 2D cluster state. Measuring the nodes marked by red in the position basis removes all edges connected to the measured nodes, and the cylindrical graph unfolds to a plane. (**B**) Resulting plane 2D cluster state after the projective measurements in (A), consisting of two bilayer square lattices (double BSL) connected by edges of weight 1/2. (**C**) Single BSL after projective measurement of half the modes in (B) in the position basis. (**D**) Square lattice (SL) after projective position measurements of all modes in spatial mode *B* (dark nodes), and applying the Fourier gate ($\pi/2$ phase delay) on half the modes in spatial mode *A* (bright nodes). This SL is a traditional universal resource state for MBQC.

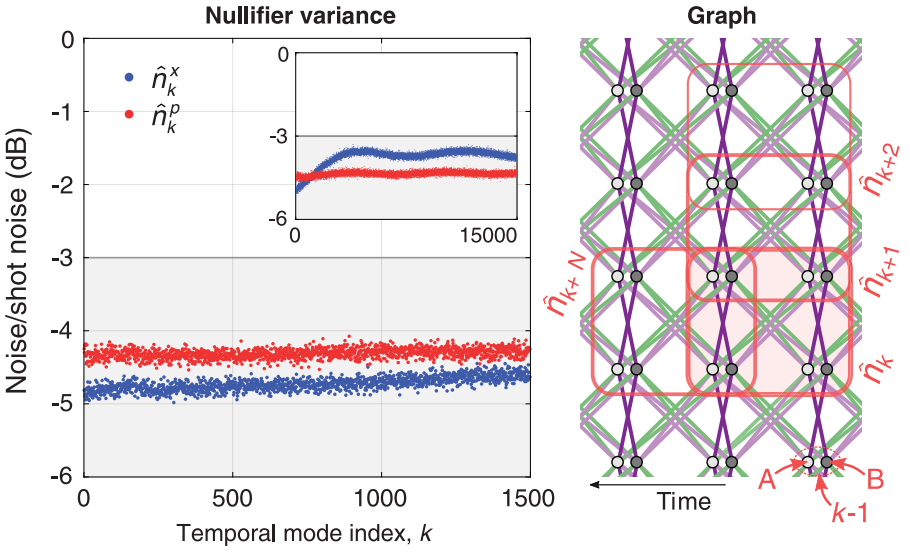

Fig. 3. Experimental result. On the right graph, the nullifiers in Eq. 1 and 2 are shown on the 2D cluster state lattice with the measured variance of 1500 consecutive nullifiers shown in the left plot. Here, the variance is calculated from 10,000 measurements of each nullifier. All nullifier variances are seen to be well below the −3-dB inseparability bound derived in supplementary text section 2 (*23*), and thus the generated cluster state is completely inseparable. In the inset, the nullifier variance of a larger data set with 2 × 15,000 = 30,000 modes is shown. Again, with all modes below the −3-dB inseparability bound, we conclude the successful generation of a 30,000-mode 2D cluster state. The rapid increase of the variance in $\hat{n}_k^x$ and its periodic variation is caused by phase fluctuation of the squeezing sources, as described in supplementary text section 4 (*23*).

index and N is the number of temporal modes in the cluster state circumference.

The practically realizable cluster state is never an exact eigenstate of the nullifiers, because such a state is unphysical. The measurement outcomes of the nullifiers are therefore not exactly zero in every measurement but possess some uncertainties around zero. A condition for complete inseparability of the 2D cluster state [derived in supplementary text section 2 (*23*)] leads to a bound on the variances of all nullifiers of 3 dB squeezing below the shot noise level. Therefore, to witness full inseparability, we must observe more than 3-dB squeezing for all nullifiers. In Fig. 3, the measured nullifier variances are shown for a dataset of 1500 nullifiers, and they are all observed to be well below the −3-dB bound; we measure an averaged variance of −4.7 and −4.3 dB for $\hat{n}_k^x$ and $\hat{n}_k^p$, respectively. In the inset of Fig. 3, we present the measurement of a longer cluster state of 15,000 temporal modes, which corresponds to a measurement time of 4 ms. Although phase instabilities are clearly seen to affect the performance in terms of variations of the nullifier variances, all variances stay below the −3-dB bound. The 2D cluster of 2 × 15,000 = 30,000 modes is thus fully inseparable. Not all 30,000 modes of the cluster state need to exist simultaneously when performing projective measurements for computation. Indeed, only a single temporal mode of the cluster state needs to exist while the remaining modes of the state are under construction. Hence, the cluster state can be immediately consumed for computation while being generated, with no additional state storage necessary (see supplementary text section 1.4 for a possible measurement scheme for computation on the cluster state).

With the deterministic generation of a universal 2D cluster state, we have [in parallel with Asavanant *et al.* (*26*)] constructed a platform for universal MBQC. Its scalability was demonstrated by entangling 30,000 optical modes in a 2D lattice that includes 24 input modes and allows for a computation depth of 1250 modes. Because only a few modes exist simultaneously, we are not limited by the coherence time of the light source, and thus the number of operations depends only on the phase stability of the system. Unlimited computational depth can therefore be achieved by implementing continuous feedback control of the system for phase stabilization, as demonstrated for the 1D photonic cluster state in (*11*). The results presented here and in (*26*) are similar: Both 2D cluster states are generated deterministically in the CV regime with comparable size and amount of squeezing in the nullifier variance. However, with only two squeezing sources, three interference points, and operation in fiber, the experimental setup demonstrated here is simpler, whereas in (*26*), larger-bandwidth OPOs are demonstrated that result in shorter delay lines. In both systems, the number of input modes can be readily increased by using OPOs with larger bandwidths, possibly combined with a longer time delay of the second interferometer. For example, using OPOs with a 1-GHz bandwidth (65 times wider) and an interferometer delay that is twice as long, a state with ~1500 input modes can be generated. Large-bandwidth OPOs have been demonstrated, but phase stability and losses in the delay lines are more challenging. Although phase fluctuation depends only on experimental control, which we expect to improve with continuous phase stabilization, delay losses are unavoidable, and increasing the OPO bandwidth may be a better solution than increasing the delay lengths.

CV cluster states are described by Gaussian statistics, but it is known that an element (state, operation, or measurement) of non-Gaussian quadrature statistics is required for universal quantum computing (*27*). Such an element could be a photon number-resolving detector (PNRD) or an ancillary cubic-phase state (*21*, *28*). Despite recent experimental efforts in developing high-efficiency PNRD (*29*) and deterministically generating optical states with non-Gaussian statistics (*30*), the formation of the required non-Gaussianity of the cluster state still constitutes an important challenge to be tackled in the future. Another currently limiting factor to achieving quantum computation is the existence of finite squeezing in the cluster, leading to excess quantum noise and thus computational errors. However, these errors can be circumvented using Gottesman-Kitaev-Preskill (GKP) state encoding (*28*) concatenated with traditional qubit error correction schemes, leading to fault-tolerant computation with a 15- to 17-dB squeezing threshold (*31*). Another recently discovered advantage of the GKP encoding is that in addition to fault tolerance, it also allows for universality without adding extra non-Gaussian states or operations (*32*). Although GKP states have recently been produced in the microwave regime (*33*) and in trapped-ion mechanical oscillators (*34*), their production in the optical regime remains a task for future work. [For further discussion on quantum computation using the generated cluster state, see supplementary text section 1.4 (*23*).] Although a path toward fault-tolerant universal quantum computing using CV cluster states has been established, it is highly likely that the first demonstrations of CV quantum computation will be nonuniversal algorithmic subroutines such as boson sampling and instantaneous quantum computing (*35*). With the large, but noisy, cluster state demonstrated here, interesting future work will be to implement basic Gaussian circuits and investigate, for example, the attainable circuit depth. Furthermore, the technique of folding a 1D cluster state into a 2D structure could be extended using an additional interferometer to form 3D cluster states,

which might be suitable for topologically protected MBQC.

REFERENCES AND NOTES

1. T. D. Ladd *et al*., *Nature* **464**, 45–53 (2010).
2. R. Raussendorf, H. J. Briegel, *Phys. Rev. Lett.* **86**, 5188–5191 (2001).
3. Y. Wang, Y. Li, Z. Yin, B. Zeng, *npj Quantum Information* **4**, 46 (2018).
4. O. Mandel *et al*., *Nature* **425**, 937–940 (2003).
5. B. P. Lanyon *et al*., *Phys. Rev. Lett.* **111**, 210501 (2013).
6. P. Walther *et al*., *Nature* **434**, 169–176 (2005).
7. Y. Tokunaga, S. Kuwashiro, T. Yamamoto, M. Koashi, N. Imoto, *Phys. Rev. Lett.* **100**, 210501 (2008).
8. S. Yokoyama *et al*., *Nat. Photonics* **7**, 982–986 (2013).
9. M. Chen, N. C. Menicucci, O. Pfister, *Phys. Rev. Lett.* **112**, 120505 (2014).
10. I. Schwartz *et al*., *Science* **354**, 434–437 (2016).
11. J. Yoshikawa *et al*., *APL Photonics* **1**, 060801 (2016).
12. S. E. Economou, N. Lindner, T. Rudolph, *Phys. Rev. Lett.* **105**, 093601 (2010).
13. N. C. Menicucci, *Phys. Rev. A* **83**, 062314 (2011).
14. P. Wang, M. Chen, N. C. Menicucci, O. Pfister, *Phys. Rev. A* **90**, 032325 (2014).
15. R. N. Alexander *et al*., *Phys. Rev. A* **94**, 032327 (2016).
16. C. Weedbrook *et al*., *Rev. Mod. Phys.* **84**, 621–669 (2012).
17. M. D. Reid *et al*., *Rev. Mod. Phys.* **81**, 1727–1751 (2009).
18. S. Armstrong *et al*., *Nat. Commun.* **3**, 1026 (2012).
19. N. C. Menicucci, S. T. Flammia, O. Pfister, *Phys. Rev. Lett.* **101**, 130501 (2008).
20. Y. Cai *et al*., *Nat. Commun.* **8**, 15645 (2017).
21. R. N. Alexander, S. Yokoyama, A. Furusawa, N. C. Menicucci, *Phys. Rev. A* **97**, 032302 (2018).
22. U. L. Andersen, T. Gehring, C. Marquardt, G. Leuchs, *Phys. Scr.* **91**, 053001 (2016).
23. See the online supplementary materials.
24. N. C. Menicucci, S. T. Flammia, P. van Loock, *Phys. Rev. A* **83**, 042335 (2011).
25. M. Gu, C. Weedbrook, N. C. Menicucci, T. C. Ralph, P. van Loock, *Phys. Rev. A* **79**, 062318 (2009).
26. W. Asavanant *et al*., *Science* **366**, 373–376 (2019).
27. S. D. Bartlett, B. C. Sanders, S. L. Braunstein, K. Nemoto, *Phys. Rev. Lett.* **88**, 097904 (2002).
28. D. Gottesman, A. Kitaev, J. Preskill, *Phys. Rev. A* **64**, 012310 (2001).
29. G. Thekkadath *et al*., arXiv:1908.04765 [quant-ph] (2019).
30. B. Hacker *et al*., *Nat. Photonics* **13**, 110–115 (2019).
31. B. W. Walshe, L. J. Mensen, B. Q. Baragiola, N. C. Menicucci, *Phys. Rev. A* **100**, 010301 (2019).
32. B. Q. Baragiola, G. Pantaleoni, R. N. Alexander, A. Karanjai, N. C. Menicucci, arXiv:1903.00012 [quant-ph] (2019).
33. P. Campagne-Ibarcq *et al*., arXiv:1907.12487 [quant-ph] (2019).
34. C. Flühmann *et al*., *Nature* **566**, 513–517 (2019).
35. D. Su *et al*., *Phys. Rev. A* **98**, 032316 (2018).
36. M. V. Larsen, X. Guo, C. R. Breum, J. S. Neergaard-Nielsen, U. L. Andersen, Deterministic generation of a two-dimensional cluster state. figshare (2019).

ACKNOWLEDGMENTS

We thank R. N. Alexander for useful discussion on the final manuscript and J. B. Brask for proofreading. **Funding:** The work was supported by the Danish National Research Foundation through the Center for Macroscopic Quantum States (bigQ, DNRF142) and the VILLUM FOUNDATION Young Investigator Programme (grant no. 10119). **Author contributions:** M.V.L. and U.L.A. conceived the project. J.S.N.-N., X.G., and C.R.B. designed and built the squeezing sources. M.V.L. developed the theoretical background, designed the experiment, and built the setup. M.V.L. performed the experiments and data analysis. The project was supervised by U.L.A. and J.S.N.-N. The manuscript was written by U.L.A., M.V.L., and J.S.N.-N. with feedback from all authors. **Competing interests:** The authors declare no competing interests. **Data and materials availability:** Experimental data and analysis code is available at figshare (*36*).

SUPPLEMENTARY MATERIALS

science.sciencemag.org/content/366/6463/369/suppl/DC1
Materials and Methods
Figs. S1 to S14
Table S1
References (*37*–*41*)

19 June 2019; accepted 25 September 2019
10.1126/science.aay4354

Science

Deterministic generation of a two-dimensional cluster state

Mikkel V. Larsen, Xueshi Guo, Casper R. Breum, Jonas S. Neergaard-Nielsen and Ulrik L. Andersen

Science **366** (6463), 369-372.
DOI: 10.1126/science.aay4354

Generating large-scale cluster states

The development of a practical quantum computer requires universality, scalability, and fault tolerance. Although much progress is being made in circuit platforms in which arrays of qubits are addressed and manipulated individually, scale-up of such systems is experimentally challenging. Asavanant *et al.* and Larsen *et al.* explore an alternative route: measurement-based quantum computation, which is a platform based on the generation of large-scale cluster states. As these are optically prepared and easier to handle (one simply performs local measurements on each individual component of the cluster state), such a platform is readily scalable and fault tolerant. The topology of the cluster state ensures that the approach meets the requirements for quantum computation.

Science, this issue p. 373, p. 369